Virologica Sinica 39 (2024) 821–832

Contents lists available at ScienceDirect

Virologica Sinica

journal homepage: www.keaipublishing.com/en/journals/virologica-sinica
www.virosin.org

Research Article

A novel vesicular stomatitis virus armed with IL-2 mimic for oncolytic therapy

Manman Wu [a], Yiwei Wang [a], Chuanjian Wu [a], Huang Huang [b], Xinyuan Zhou [c,*], Jun Wang [a,*], Sidong Xiong [a,*], Chunsheng Dong [a,*]

[a] The Institutes of Biology and Medical Sciences, MOE Key Laboratory of Geriatric Diseases and Immunology, Jiangsu Key Laboratory of Infection and Immunity, Soochow University, Suzhou 215123, China
[b] Department of Cardiology, No. 981 Hospital, PLA (People's Liberation Army of China), Chengde 067000, China
[c] Institute of Immunology, College of Basic Medical Sciences, Third Military Medical University, Chongqing 400038, China

ARTICLE INFO

Keywords:
Combination therapy
IL-2 mimic
Neo-2/15
Oncolytic virus (OV)
Tumor immunity
Vesicular Stomatitis virus (VSV)

ABSTRACT

Oncolytic virus (OV) is increasingly being recognized as a novel vector in cancer immunotherapy. Increasing evidence suggests that OV has the ability to change the immune status of tumor microenvironment, so called transformation of 'cold' tumors into 'hot' tumors. The improved anti-tumor immunity can be induced by OV and further enhanced through the combination of various immunomodulators. The Neo-2/15 is a newly de novo synthesized cytokine that functions as both IL-2 and IL-15. However, it specifically lacks the binding site of IL-2 receptor α subunit (CD25), therefore unable to induce the Treg proliferation. In present study, a recombinant vesicular stomatitis virus expressing the Neo-2/15 (VSV^{M51R}-Neo-2/15) was generated. Intratumoral delivery of VSV^{M51R}-Neo-2/15 efficiently inhibited tumor growth in mice without causing the IL-2-related toxicity previously observed in clinic. Moreover, treatment with VSV^{M51R}-Neo-2/15 increased the number of activated $CD8^+$ T cells but not Treg cells in tumors. More tumor-bearing mice were survival with VSV^{M51R}-Neo-2/15 treatment, and the surviving mice displayed enhanced protection against tumor cell rechallenge due to the induced anti-tumor immunity. In addition, combination therapy of OV and anti-PD-L1 immune checkpoint inhibitors further enhanced the anti-tumor immune response. These findings suggest that our novel VSV^{M51R}-Neo-2/15 can effectively inhibit the tumor growth and enhance the sensitivity to immune checkpoint inhibitors, providing promising attempts for further clinical trials.

1. Introduction

Cancer is one of the most serious diseases that threats human health and the morbidity is gradually increasing. The traditional treatments, such as surgery, chemotherapy, and radiation therapy, are effective but not enough to conquer the disease yet, so it remains a huge challenge to cure cancers. Despite the recent emergence of immune checkpoint blockade therapy (Topalian et al., 2015) and the successful application of adoptive cell therapy (Rosenberg and Restifo, 2015; Restifo et al., 2012) in clinical practice, most patients either respond poorly to these therapies or suffer from severe immune-related adverse events, including pneumonitis, pancreatitis, and colitis (Lamers et al., 2013; Michot et al., 2016). Therefore, it is urgent to explore a new tumor immunotherapy for better control of cancers.

Tumor immunotherapy mediated by oncolytic virus (OV) is considered a promising approach (Harrington et al., 2019). OV can selectively infect and replicate in tumor cells, causing the lysis of tumor cells. The release of tumor antigens, in turn, stimulates the innate and adaptive immune responses (Chaurasiya et al., 2018). Tumor cell lysate also leads to the release of viral pathogen-associated molecular patterns (PAMPs), cellular damage associated molecular patterns (DAMPs), and cytokines (such as IFN-γ, TNF-α, and IL-12), which elevate the immune responses (Goradel et al., 2021). Talimogene laherparepvec (T-Vec), an attenuated type I herpes simplex virus encoding granulocyte-macrophage colony stimulating factor (GM-CSF), is the first OV approved by FDA in 2015 for the treatment of unresectable melanoma (Johnson et al., 2015). In a phase III clinical trial, the intratumoral injection of T-Vec into melanoma tumor improved the durable response rate compared with GM-CSF

* Corresponding authors.
E-mail addresses: chunshengdong@suda.edu.cn (C. Dong), sdxiong@suda.edu.cn (S. Xiong), jwang79@suda.edu.cn (J. Wang), xinyuanzhou@tmmu.edu.cn (X. Zhou).

https://doi.org/10.1016/j.virs.2024.09.007
Received 16 February 2024; Accepted 11 September 2024
Available online 17 September 2024

treatment (16.3% vs. 2.1%). The objective response rate and complete response rate with T-Vec were 26.4% and 10.8%, respectively (Hamid et al., 2020). Vesicular stomatitis virus (VSV) is a single-stranded, negative sense RNA virus, comprised of five genes and belonging to the *Rhabdoviridae* family. Because the natural hosts of this virus are Artiodactyla animals, the symptoms caused by viral infection in humans are mild or asymptomatic (Bishnoi et al., 2018). The virus is extremely sensitive to interferon, which is defective in most tumor cells, making it an ideal OV for selective eradication of tumor cells (Stojdl et al., 2000). Numerous preclinical studies have demonstrated that VSV is a promising OV for various malignancies, including melanoma (Galivo et al., 2010), colorectal cancer (Gray et al., 2019), hepatocellular carcinoma (Ebert et al., 2003), breast cancer (Ahmed et al., 2010), prostate cancer (Udayakumar et al., 2020), and glioblastoma (Cary et al., 2011). Different types of engineered VSVs have been used in clinical trials (see details at ClinicalTrials.gov for trials NCT01628640, NCT03120624, NCT02923466, NCT03865212, NCT03017820, NCT03647163, and NCT04787003). These modified VSVs, such as the incorporation of immunostimulatory cytokines GM-CSF, IL-2, and IL-12, chemokines CCL5, CCL19, CCL20, and CCL21, immune-activating ligands CD40L and OX40L (Markert et al., 2012; Amedei et al., 2013; Li et al., 2016; Ylosmaki et al., 2021), greatly boost potent anti-tumor responses.

IL-2 is a T cell growth factor predominantly secreted by activated T cells (Morgan et al., 1976). IL-2 stimulates the activation and proliferation of immune cells through receptor complexes, comprising IL2Rα (CD25), IL2Rβ (CD122), and the co-receptor IL-2Rγ (CD132) chains (Wang et al., 2005). The effect of IL-2 binding with its receptor is multidirectional. The downstream signaling of the IL-2Rβγ heterodimer with the binding of a high dose of IL-2 can induce the expansion of tumor-killing CD8 T cells. However, IL-2 also has a much high affinity for IL-2Rα, which is constitutively expressed by $CD4^+$ $FoxP3^+$ Treg cells. Therefore, a lower amount of IL-2 is required for the IL-2Rαβγ complex to bind and expand the immunosuppressive Treg cell (Boyman and Sprent, 2012). High-dose of IL-2 was approved as a standard immunotherapy regimen for the treatment of metastatic melanoma and kidney cancer in the 1980s (Rosenberg, 2001). Side effects like vascular leak syndrome, hypotension, and liver toxicities associated with high dose of IL-2 hinder its clinical application (Marabondo and Kaufman, 2017). Moreover, the potently suppressive $CD4^+CD25^+FoxP3^+$ Treg cells in patients increased with high dose of IL-2 (Ahmadzadeh and Rosenberg, 2006). In view of this, a variety of modified IL-2, such as PEG-IL-2 and IL-2-Fc, has been developed to overcome these problems (Abbas et al., 2018; Sharma et al., 2020). Recently, an IL-2 mimic (Neo-2/15) was synthesized, which does not contain the binding site of IL-2Rα chain, but still retains the ability to bind to the IL-2Rβγ complex. This IL-2 mimic has a long half-life, lower toxicity, and preferential activation of cytotoxic $CD8^+$ T lymphocyte instead of Tregs (Silva et al., 2019).

In addition to having a direct oncolytic effect at tumor site, OVs have been extensively used as a platform to deliver cytokines or other therapeutic agents to enhance the immune response. In this study, to further improve the local immune microenvironment and promote the therapeutic effects of OV, we armed a recombinant VSV with the novel IL-2 mimic Neo-2/15 and investigated its antitumor effect in mouse tumor models.

2. Materials and methods

2.1. Mice and cells

6–8 weeks old female C57BL/6J mice and BALB/c mice were purchased from Selleck (Shanghai, China). All mice were housed in Animal Biosafety Level 2 Laboratory. All animal experiment protocols in this study were approved by the Ethics Committee of Soochow University.

The human embryonic kidney cell line (HEK293T), baby hamster kidney fibroblast cell line (BHK-21), Lewis lung cancer cell (LLC), and African green monkey kidney cell line (Vero) were purchased from National Collection of Authenticated Cell Cultures (Shang Hai, China). Mouse colon cancer cell line (MC-38) was a gift from Prof. Yunsen Li. These cells were cultured in Dulbecco's Modified Eagle Medium (Hyclone, USA) supplemented with 10% fetal bovine serum (Hyclone) and 100 units/mL penicillin/streptomycin (Invitrogen, USA) in a 5% CO_2 incubator at 37 °C.

2.2. Construction of recombinant VSVs

The Neo-2/15 sequence was obtained as described (Silva et al., 2019) and synthesized by GENEWIZ (Suzhou, China). The Neo-2/15 DNA fragment was then cloned into the vector pXN_2-M51R, which encodes the full-length of VSV genome, to generate pXN_2-Neo-2/15. Recombinant viruses were rescued in BHK-21 cells using a reverse genetics approach. Briefly, BHK-21 cells were first infected with a vaccinia virus expressing the T7 RNA polymerase, then transfected with pXN_2-Neo-2/15 together with pP, pN, and pL plasmids via Lipofect 2000 (Invitrogen). The cell culture medium was collected, and vaccinia virus was removed by filtration through a 0.22 μm filter 48 h post transfection. The VSV^{M51R}-mIL-2 expressing mouse IL-2 was generated by a similar procedure. The VSV^{M51R}-GFP was generated as described in a previous study (Wu et al., 2019). These recombinant VSVs were amplified in Vero cells and purified by gradient centrifugation with sucrose density of 55%, 40%, and 25%. Virus titre was determined by $TCID_{50}$ on Vero cell monolayers and calculated by the Reed-Muench method.

2.3. Viral replication assay in vitro

Vero cells were seeded at 1.0×10^5 per well in six-well plates and infected the next day with the indicated viruses at an MOI of 0.1 in 1 mL medium containing 2% FBS. The culture supernatants were collected at 24, 36, 48, and 72 h post infection and the supernatant titers were determined by $TCID_{50}$ assay.

2.4. Western blot analysis

Vero cells were collected 48 h post infection and lysed with RIPA buffer containing 1 mM protease inhibitor PMSF. Cellular proteins were separated by 10% SDS-polyacrylamide gel electrophoresis and transferred to a polyvinylidene fluoride membrane. After blocking with PBS containing 0.1% Tween-20 (PBST) and 5% fat-free milk, the membranes were incubated with the primary antibodies anti-Flag (Sigma, USA, 1:2000) at 4 °C overnight. After washing with PBST three times, the membranes were incubated with horseradish peroxidase (HRP)-conjugated secondary goat anti-rabbit IgG (Sigma, USA, 1:5000) for 2 h at room temperature. Detection was performed with enhanced chemiluminescence (Pierce, USA).

2.5. Cytotoxicity assay

Tumor cells were plated at 1.0×10^4 cells per well in 96-well plates and infected the next day with the indicated viruses at an MOI of 1 or 10. Cell viability was determined 48 h post infection using CCK-8 kit (MCE, China) according the manufacturer's protocol.

2.6. Detection of Neo-2/15 using relative ELISA assay

To detect Neo-2/15 expressed in the viral supernatants, a 96-well plate was coated with viral supernatant at 4 °C overnight. Coated plate was incubated with blocking buffer at room temperature for 1 h. After three times washing, the plate was then incubated with a home-made mouse anti-Neo-2/15 serum at 1:1000 dilution at room temperature for 2 h. After three times washing, binding was detected with HRP-conjugated anti-mouse IgG antibody and developed with 3,3′,5,5-tetramethylbenzidine (TMB) using the absorption at 450 nm.

2.7. Animal experiments

MC-38 cells (7×10^5) or LLC cells (4×10^5) were inoculated subcutaneously (s.c.) into the right forelimb underarm of each C57BL/6J female mouse. Tumor sizes (width and length) were measured every two days by a vernier caliper. Tumor volume (V) was calculated by the formula: $V = 0.5 \times L \times W^2$ (L = length; W = width). When the tumor volume reached 40–50 mm^3, 1×10^8 pfu virus or PBS was injected into the tumors every two days for a total of three times. Mice were euthanized when tumor volume reached approximately 2000 mm^3. For combination therapy, anti-PD-L1 monoclonal antibody was purchased from Bio X cell (Clone#10F.9G2, USA), and was injected intraperitoneally at 100 μg per mouse every two days for a total of three injections. In rechallenge studies, the cured mice, previously treated with VSV^{M51R}-Neo-2/15 and surviving for more than three months, were rechallenged (s.c.) with 4×10^5 MC-38 cells. Naïve mice also received 4×10^5 MC-38 cells as a control. Tumor size was measured over time. The spleens of rechallenged mice were collected and processed into a single cell suspension 21 days post inoculation. The dissociated cells were further stained for flow cytometric assessment of $CD8^+$, $CD62L^+$, and $CD44^+$ by FACS.

2.8. Flow cytometry

Excised tumors were minced and digested using a mixture of collagenase IV (Worthington, USA) and DNase I (Roche, Switzerland) in a shaker for 30 min, 250 rpm. at 37 °C. After digestion, samples were passed through a 70-μm cell strainer, and resuspended in cold complete RPMI 1640 medium, supplemented with 10 mM HEPES buffer, 1 mM sodium pyruvate, 50 μM 2-mercaptoethanol, 100 U/mL penicillin and 100 μg/mL streptomycin and complemented with 1% non-essential amino acids (NEAA), 1% GlutaMAX supplement and 10% heat-inactivated FBS. The cell suspensions from the spleens were obtained by smashing the tissues and passing it through a 70-μm cell strainer. Red blood cells were removed by incubation with ACK lysis buffer (Thermo Fisher, USA). Spleen cells were resuspended in PBS with 2% FBS and 1 mM EDTA, and stained for extracellular markers for 45 min at 4 °C. Cell suspensions were then fixed, permeabilized and stained for intracellular markers using the eBioscience FoxP3 Transcription Factor Staining Buffer Set (Thermo Fisher). The following antibodies and dilutions were used for flow cytometric analysis: CD45-APC (BD Biosciences, USA, 1:200), CD8-Percp (BD Biosciences, 1:200), CD8-APC (BD Biosciences, 1:200), CD4-FITC (BD Biosciences, 1:200), CD62L-PE (BD Biosciences, 1:200), CD44-Alexa Fluor 488 (BD Biosciences, 1:200), FoxP3-PE (eBioscience, USA, 1:100), and IFN-γ-PE (BD Biosciences, 1:100). Samples were measured on a FACS Canto II cytometer (BD Biosciences), and data were analyzed using FlowJo v.10 software.

2.9. Quantitative PCR

Tumors were collected one day post the last treatment and digested into single-cell suspension. $CD8^+$ T cells were sorted by EasySep T Cell Isolation Kit (StemCell Technologies, Canada), and total RNA was extracted from $CD8^+$ T cells and reverse transcribed into cDNA. Quantitative PCR was performed using 5 × PowerUp SYBR Green Master Mix (ABI, USA) and QuantStudio Q6 Flex to measure the mRNA levels of genes. All primers for the analysis were purchased from Genwiz. The following pairs of primers were used (GAPDH: Forward, 5′-GAGCCAAACGGGTCATCATCT-3′; GAPDH reverse, 5′-GAGGGGCCATCCACAGTCTT-3′; Granzyme B:Forward, 5′-CCTGCTACTGCTGACCTTGT-3′; Granzyme B reverse: 5′-AGGCTGCTGATCCTTGATCG-3′; Perforin: Forward, 5′-CAAGCCTCTCCGTGGTTGTC-3′; Perforin reverse, 5′-GCTGCAGGCACAGTAGTCAT-3′; TNF-α:Forward, 5′-CCTGTAGCCCACGTCGTAG-3′; TNF-α reverse, 5′-GGGAGTAGACAAGGTACAACCC-3′; PD-L1: Forward, 5′-GCTCCAAAGGACTTGTACGTG-3′; PD-L1 reverse, 5′-TGATCTGAAGGGCAGCATTTC-3′). Relative gene expression normalized to GAPDH was determined by the $2^{-\Delta\Delta CT}$ method.

2.10. T cell proliferation assay

$CD8^+$ T cells were isolated from mice spleens using the EasySep T Cell Isolation Kit (StemCell Technologies). Cells were plated in RPMI in 96-well culture plates at a density of 20,000 cells/well. Medium was supplemented with mouse IL-2 (10 ng/mL) or 20 μL of VSV^{M51R}-GFP, VSV^{M51R}-mIL-2, or VSV^{M51R}-Neo-2/15 infected cell medium. Cell numbers were measured by flow cytometry 3 days after incubation.

2.11. NK cell proliferation assay

For primary NK cells, NK cells were isolated from mice spleen cells stained with $CD3^-NK1.1^+$ using FACS sorting. Cells were plated in 96-well culture plates at a density of 10,000 cells/well. Medium was supplemented with mouse IL-2 (10 ng/mL) or 20 μL of VSV^{M51R}-GFP, VSV^{M51R}-mIL-2, or VSV^{M51R}-Neo-2/15 infected cell medium. Cells numbers were measured by flow cytometry 3 days post incubation.

2.12. Lymphocyte cytotoxicity assay

$CD8^+$ T cells and NK cells were purified from mice spleen cells as described above, and $CD8^+$ T cells were stimulated with anti-CD3/CD28 antibodies for 24 h, then $CD8^+$ T cells or NK cells were plated in 96-well culture plates at a density of 100,000 cells/well. The medium was supplemented with mIL-2 (10 ng/mL), or 20 μL VSV^{M51R}-GFP, VSV^{M51R}-mIL-2, or VSV^{M51R}-Neo-2/15 infected cell medium. After 3 days, the cells were washed with PBS, and then cocultured with 20,000 MC-38 cells for 2 days. The cytotoxicity of effector cells was measured by a CCK-8 kit.

2.13. Assessment of treatment-related toxicity

Virus-treated mice were sacrificed 4 to 5 days post treatments for blood, kidneys, and lungs collections. Blood samples were kept for 30 min at 37 °C, and sera were separated by centrifugation for measurement of alanine transaminase (GOT) and aspartate transaminase (GPT) using commercially available kits (Solarbio, China) according to manufacture instructions. Water content was used to monitor tissue oedema. Briefly, wet tissues were weighed and dehydrated overnight above 100 °C in a chemical hood. The difference in weight between wet and dry tissues was calculated.

2.14. Statistical analyses

All statistical analyses were performed using GraphPad Prism 9. Data are presented as the mean ± SD. Student's *t*-test was used for unpaired comparisons of two groups. Differences between more than two groups were determined by one-way analysis of variance (ANOVA), and the Kaplan-Meier method with the log-rank test was used for survival analysis. $P < 0.05$ was considered significant.

3. Results

3.1. Construction of recombinant VSV expressing Neo-2/15

The VSV carrying M51R mutation in matrix protein is attenuated and applied as an oncolytic virus vector (Bishnoi et al., 2018). To construct VSV^{M51R}-mIL-2 and VSV^{M51R}-Neo-2/15, mIL-2 and Neo-2/15 coding sequences were inserted into the G and L genes of VSV^{M51R}, respectively (Fig. 1A). The recombinant viruses were recovered by transfection of the plasmid encoding full-length VSV genome together with pP, pN, pL helper plasmids into BHK cells as previously described (Lawson et al., 1995). We next determined whether the recovered VSVs expressed mIL-2 or Neo-2/15. Accordingly, Vero cells were infected with VSV^{M51R}-mIL-2

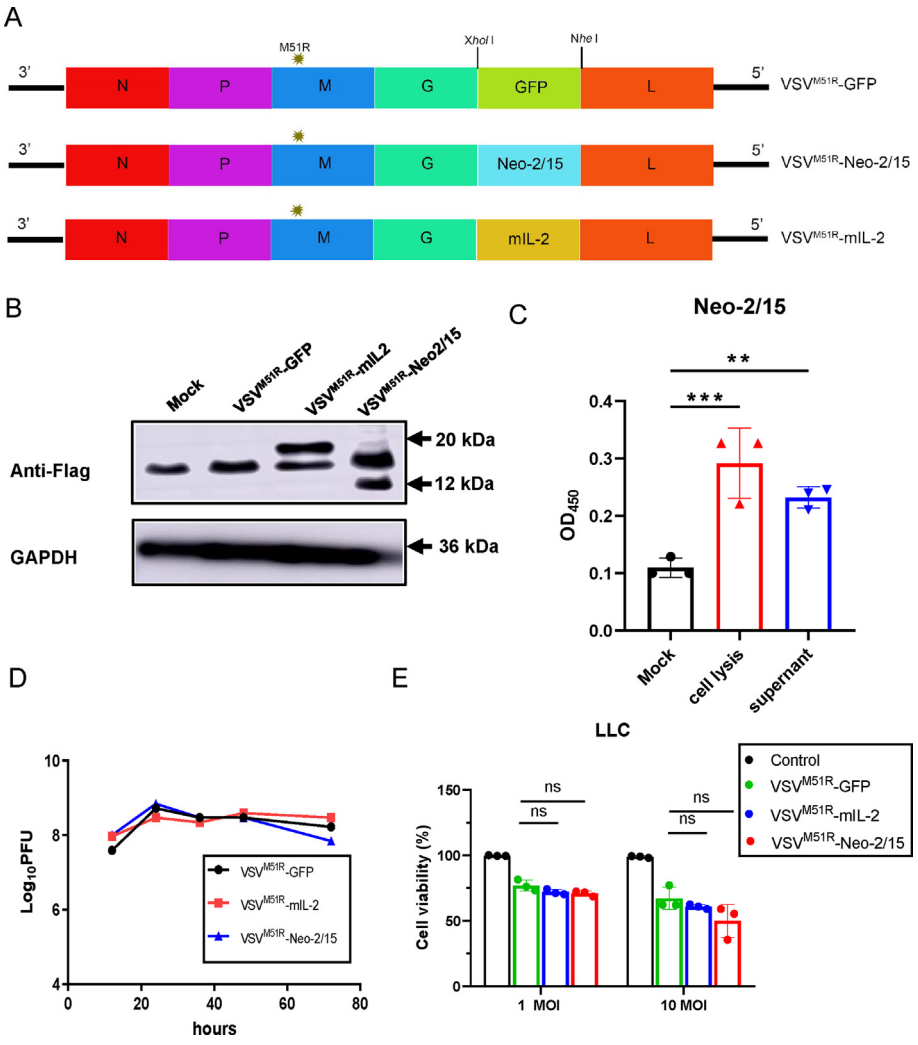

Fig. 1. Construction and characterization of VSVs. **A** Schematic genome structure of recombinant viruses. **B** The expression of mIL-2 and Neo-2/15 were detected by Western blot. Vero cells were infected with VSV^{M51R}-mIL-2 or VSV^{M51R}-Neo-2/15 (MOI = 0.1) for 48 h. The cell lysate was collected for Western blot using anti-flag antibody. **C** The expression of Neo-2/15 in the infection supernatant and cell lysate was detected using relative ELISA. **D** Replication curves of recombinant VSVs. Vero cells were infected with indicated viruses at MOI = 0.1. The viral titers in the supernatants at different time points were measured by $TCID_{50}$ assay. **E** Cytotoxicity of recombinant VSVs. MC-38 cells was infected with viruses at an MOI of 1 or 10. Cell viability was measured at 48 h by CCK-8 kit. Data are represented as the mean ± SD. One way ANOVA test was used for non-paired comparisons of multiple groups. $^{**}P < 0.01$; $^{***}P < 0.001$; ns: no significance.

or VSV^{M51R}-Neo-2/15 for 48 h at an MOI of 0.1. Infected cells were examined for mIL-2 or Neo-2/15 expression by immunoblot analysis using an anti-Flag antibody. Our results indicated that the mIL-2 and Neo-2/15 protein were expressed in infected cells at the predicted molecular weight, while no mIL-2 or Neo-2/15 expression was detected in uninfected cells (Fig. 1B). In addition, the expression of Neo-2/15 in supernatant was confirmed by relative ELISA (Fig. 1C). To compare the replication efficiency of the recombinant viruses with VSV^{M51R}-GFP control, Vero cells were infected with VSV^{M51R}-GFP, VSV^{M51R}-mIL-2, or VSV^{M51R}-Neo-2/15 at an MOI of 0.1, and the viral titers in supernatants were determined at different time points post infection. Our data indicated that these three viruses exhibited similar replication kinetics (Fig. 1D). To evaluate whether the recombinant viruses retained their ability to kill tumor cells, mouse colon cancer cell line MC-38 cells were infected with recombinant VSVs and the cell viability of MC-38 cells were analyzed after infection. The results indicated that the oncolytic activities of the three viruses were not significantly different (Fig. 1E).

3.2. *Functional characterization of Neo-2/15 expressed by VSV^{M51R}-Neo-2/15*

IL-2 is a growth factor for T cells. To determine the biological activity of Neo-2/15 expressed by VSV^{M51R}-Neo-2/15, we sorted CD8$^+$ T cells and NK cells from mouse spleen cells and cultured them in the viral supernatant containing medium for 3 days. As expected, the viral supernatant of VSV^{M51R}-Neo-2/15 promoted the survival and proliferation of both mouse CD8$^+$ T and NK cells (Fig. 2A and B). However, due to the lack of IL-2 in control or VSV^{M51R}-GFP culture medium, the sorted CD8$^+$ T cells succumbed to death and the cell number was less than the initial input (2×10^4). In addition, CD8$^+$ T and NK cells activated by VSV^{M51R}-Neo-2/15 effectively killed tumor cells *in vitro* (Fig. 2C and D). In order to determine whether VSV^{M51R}-Neo-2/15 induced Treg cell proliferation, we isolated conventional naïve CD4$^+$ T cells from mouse spleens and cultured them in the presence of VSV^{M51R}-Neo-2/15 supernatant for 3 days. As shown in Fig. 2E, the percentage of CD4$^+$ FoxP3$^+$ Treg cells induced by

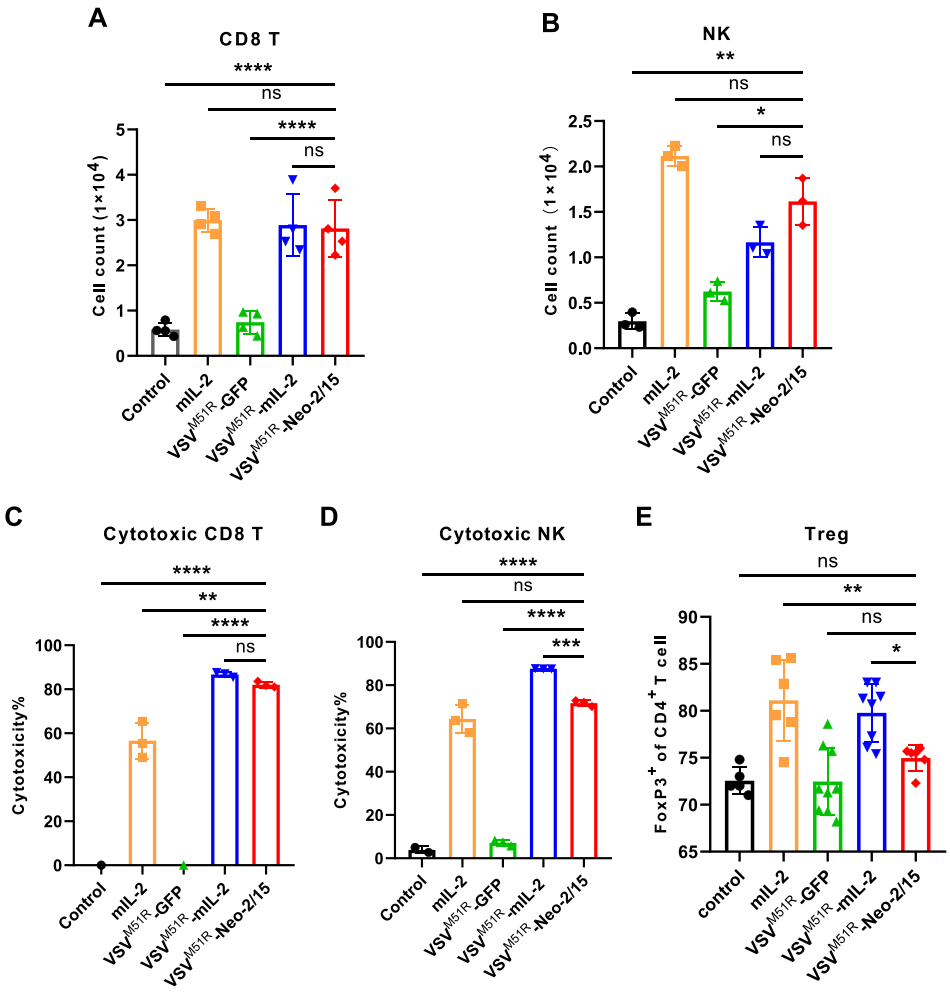

Fig. 2. Functional characterization of VSV^{M51R}-Neo-2/15 *in vitro*. **A** Survival and proliferation of CD8$^+$ T cells. CD8$^+$ T cells were purified from mice spleen cells and plated in 96-well plates at a density of 20,000 cells/well. The culture medium was supplemented as indicated. After 3 days, cell numbers were measured by FACS. **B** Survival and proliferation of NK cells. CD3-NK1.1$^+$ NK cells were purified from mice spleen cells by FACS sorting. Cells were plated in 96-well culture plates at a density of 10,000 cells/well. The culture medium was supplemented as indicated. After 3 days, cell numbers were measured by FACS. **C** CD8$^+$ T cells were purified from mice spleen cells and stimulated with anti-CD3/CD28 antibodies for 24 h. Then the CD8$^+$ T cells were plated in 96 well culture plates at a density of 100,000 cells/well supplemented as indicated containing medium for 3 days. The cells were further cocultured with 20,000 MC-38 cells for 2 days. The cytotoxicity of CD8$^+$ effector cells were measured by CCK-8 kit. **D** Activated NK cells were cocultured with MC-38 cells. After 48 h, cytotoxicity of NK effector cells was measured by CCK-8 kit. **E** The differentiation of FoxP3$^+$ CD4$^+$ Tregs. Conventional CD4$^+$ T cells were purified and plated in 24 well plates (5.0×10^5 cells/well) with anti-CD3 antibody (pre-coated, 0.5 μg/mL), CD28 (0.5 μg/mL), TGF-β (0.5 ng/mL). In addition, the cell culture was supplied with viral supernatants or mIL-2 (10 ng/mL), control group with no added. The percentage of FoxP3$^+$ CD4$^+$ T cells were measured by FACS 3 days post plating. Data are represented as the mean ± SD. One way ANOVA test was used for non-paired comparisons of multiple groups. *$P < 0.05$; **$P < 0.01$; ***$P < 0.001$; ****$P < 0.0001$; ns: no significance.

VSV^{M51R}-Neo-2/15 supernatant was lower than that of mIL-2 and VSV^{M51R}-mIL-2 supernatant groups, suggesting the inefficiency of VSV^{M51R}-Neo-2/15 in inducing Treg cells. Altogether, our data indicate that VSV^{M51R}-Neo-2/15 has been successfully engineered to express Neo-2/15 with biological activity.

3.3. VSV^{M51R}-Neo-2/15 exhibits better therapeutic effects in mouse cancer model

In order to evaluate the therapeutic effects of VSV^{M51R}-Neo-2/15 in mice, mice colon tumor cell MC-38 was used to generate a tumor-bearing model. On day 9 post MC-38 inoculation, tumor-bearing mice were randomly divided into four groups, which were subsequently intratumorally injected with 1×10^8 pfu virus or PBS (Fig. 3A). We then monitored tumor growth every two days and found that tumors in PBS group grew rapidly and the average volume reached 1069 mm^3 on day 19 post inoculation. Compared with the PBS-treated tumors, the inhibition efficiency of tumor growth was 47.4% for treatment with VSV^{M51R}-GFP (562.3 mm^3), 65.9% with VSV^{M51R}-mIL-2 (363.6 mm^3), and 82.2% with VSV^{M51R}-Neo-2/15 (188.8 mm^3) (Fig. 3B and C). PBS-treated mice began to succumb to tumor progression on day 15, and all died on day 23. While mice treated with VSVs survived longer than the PBS group, and eventually VSV^{M51R}-Neo-2/15-treated mice had an enhanced survival rate of 40%, with four mice being completely cured (Fig. 3D). Similar results were observed in mouse Lewis lung cancer model (Supplementary Fig. S1). Taken together, these results indicated that VSV^{M51R}-Neo-2/15 could significantly inhibit tumor growth and prolong the survival time of tumor-bearing mice.

Currently, the toxicity caused by high-dose IL-2 treatment is one of the main reasons preventing its use in clinical (Siegel and Puri, 1991; Blattman et al., 2003). Mouse serum alanine transaminase (GOT) and aspartate transaminase (GPT) were detected one day post the last

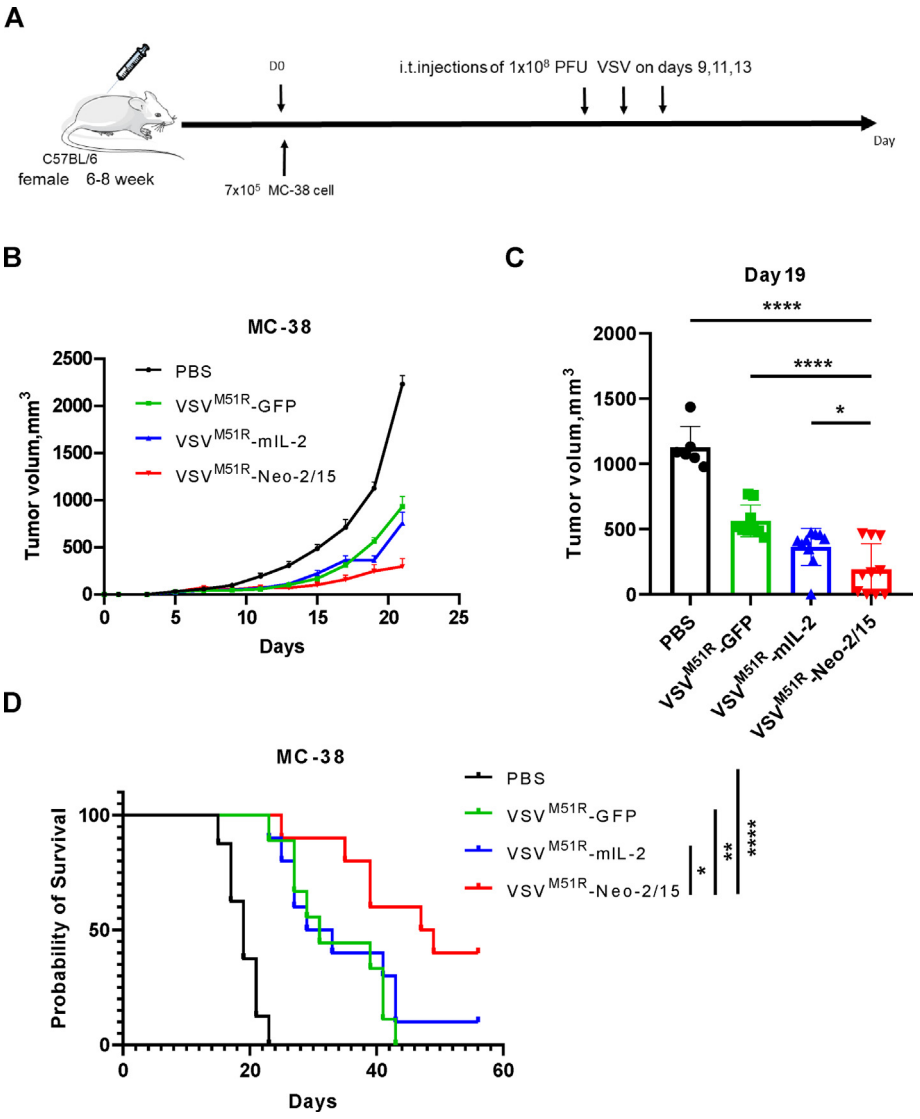

Fig. 3. Therapeutic effects of VSV^{M51R}-Neo-2/15 on colon tumor model. **A** MC-38 cells (7.0×10^5) were implanted into the flank of C57BL/6 mice. Tumor-bearing mice were subjected to mock treatment (n = 8) or intratumoral injections of 1.0×10^8 pfu VSV^{M51R}-GFP (n = 9), VSV^{M51R}-mIL-2 (n = 10), VSV^{M51R}-Neo-2/15 (n = 10) every 2 days for a total of 3 times starting from day 9. **B** Tumor volumes were determined every 2 days. **C** The tumor volume of each group on day 19 post-implantation. **D** Survival rate of each treated group mice. Data are represented as the mean ± SD. One way ANOVA test was used for non-paired comparisons of multiple groups. The Kaplan-Meier method with the log-rank test was used for survival analysis. $^*P < 0.05$; $^{**}P < 0.01$; $^{****}P < 0.0001$.

treatment. Liver and lung organs were also collected to assess tissue oedema, a hallmark of IL-2-induced vascular leakage syndrome. Serum GPT and GOT increased only in hIL-2-treated group (Fig. 4A and B). Similarly, these mice had increased water content in the liver and lung organs (Fig. 4C and D), suggesting that VSV^{M51R}-Neo-2/15 treatment does not induce pulmonary and hepatic oedema.

3.4. VSV^{M51R}-Neo-2/15 promotes anti-tumor immune memory responses

To determine whether memory T cells were potentiated in the cured mice, we rechallenged the mice that survived for more than three months with 4×10^5 MC-38 cells. As shown in Fig. 5A, only one mouse (n = 6) formed a tumor, but it progressed slowly. Three weeks after tumor rechallenge, spleens from cured mice were collected, and the proportion of CD8$^+$ central memory (CD44$^+$ CD62L$^+$) T cells was significantly increased in VSV^{M51R}-Neo-2/15 cured mice compared to normal mice (Fig. 5B). Moreover, when co-cultured with MC-38 cells, spleen cells from cured mice could effectively kill MC-38 cells (Fig. 5C). Collectively, these results indicated that VSV^{M51R}-Neo-2/15 treatment is able to enhance long-term anti-tumor memory immune responses that effectively prevent the growth of tumor cells upon rechallenge.

3.5. VSV^{M51R}-Neo-2/15 preferentially activates and expands CD8 T cells rather than Treg cells

Tumor-infiltrating lymphocytes were collected 24 h after the last treatment and analyzed by flow cytometry. Either the number of CD8$^+$ T cell or the percentage of CD8$^+$ T cells increased with VSV^{M51R}-Neo-2/15 treatment in comparison to other treatments (Fig. 6A and B). The number and percentage of cytotoxic CD8$^+$ T cells (IFN-γ$^+$ CD8$^+$ T) also increased in VSV^{M51R}-Neo-2/15 group (Fig. 6C and D). IL-2 administration has been found to increase CD4$^+$CD25$^+$FoxP3$^+$ Treg cells in cancer patients (Ahmadzadeh and Rosenberg, 2006). The high infiltration of Treg into tumor tissue leads to poor survival of patients with various types of cancer (Togashi et al., 2019). Notably, we did not observe a significant increase in Treg cells (CD4$^+$ FoxP3$^+$) in this study (Fig. 6E and F).

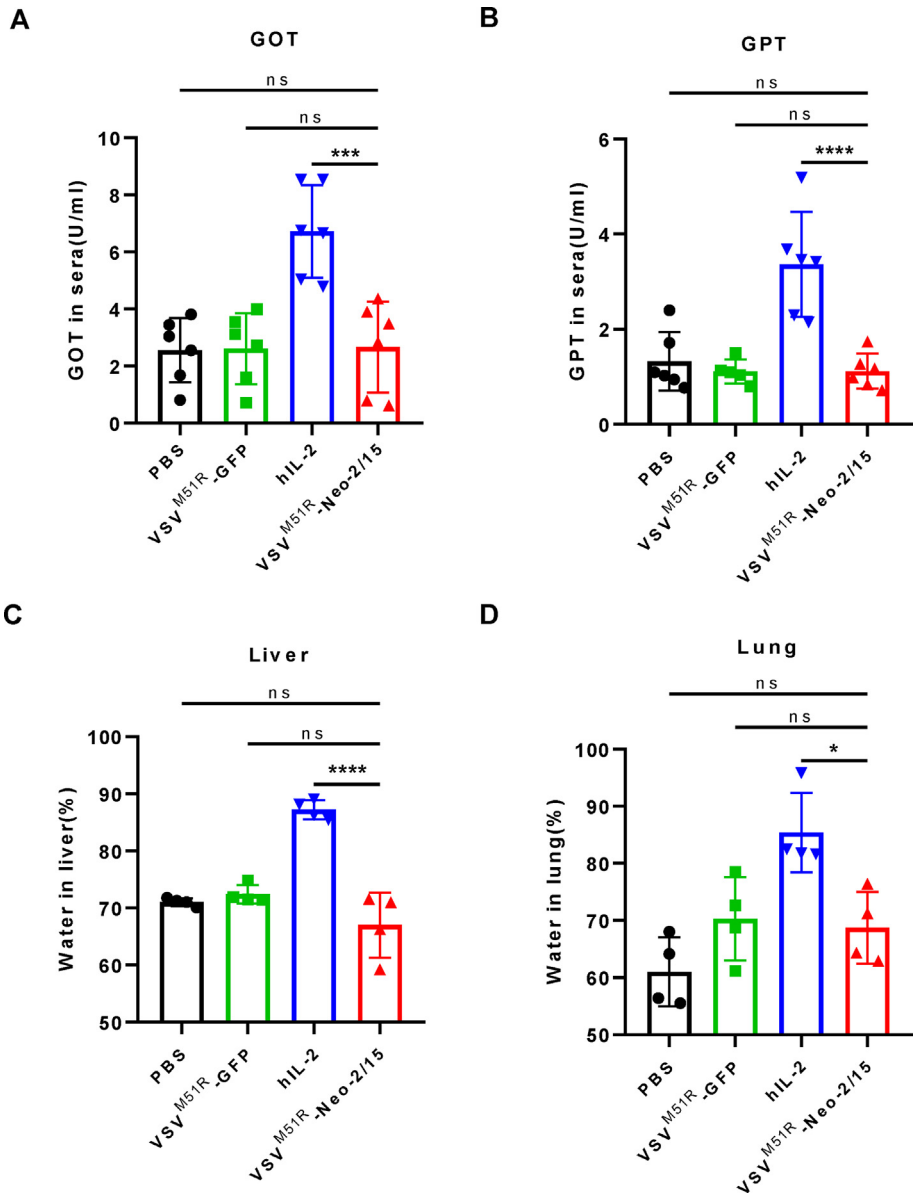

Fig. 4. The toxicity of VSV^{M51R}-Neo-2/15 therapy. Tumor-bearing mice were injected intratumorally (i.t.) with VSVs (1×10^8 pfu/mouse) every 2 days for a total of 3 times, or intraperitoneal injection (i.p.) injected with hIL-2 (500,000 U) every day and for a total of 6 times. The lung, liver and serum were collected after the last injection of virus or hIL-2 on day 6. Serum alanine transaminase (GOT, **A**) and aspartate transaminase (GPT, **B**) in serum and water in liver (**C**) and lung (**D**) were measured. Data are represented as the mean ± SD. One way ANOVA test was used for non-paired comparisons of multiple groups. *$P < 0.05$; ***$P < 0.001$; ****$P < 0.0001$; ns: no significance.

Moreover, the ratio of CD8$^+$ T/Treg was higher in VSV^{M51R}-Neo-2/15 group (Fig. 6G). Furthermore, we found that the expression level of Granzyme B, perforin and TNF-α was higher in infiltrating CD8$^+$ T cells in VSV^{M51R}-Neo-2/15-treated group compared with that of other counterparts (Fig. 6H). These results suggest that VSV^{M51R}-Neo-2/15 therapy preferentially expands CD8$^+$ T cells rather than immunosuppressive Treg cells in tumor milieu.

3.6. *Immune checkpoint inhibitor enhances therapeutic effects of VSV^{M51R}-Neo-2/15*

Immune checkpoint inhibitors such as PD-1 and PD-L1 antibodies have achieved excellent clinical results (Lin et al., 2018; Tumeh et al., 2014). Interestingly, we found that PD-L1 expression was up-regulated *in vitro* and *in vivo* (Fig. 7A and B), implying a better efficacy of VSV^{M51R}-Neo-2/15 and PD-L1 antibody combination therapy. We then verified the anti-tumor effect of VSV^{M51R}-Neo-2/15 combined with PD-L1 antibody in mouse model (Fig. 7C). Mice were injected intratumorally with virus and intraperitoneally with anti-PD-L1 antibody three times when the tumor volume reached about 50 mm^3. Compared to the monotherapy group, tumor growth of combination therapy was delayed (Fig. 7D). The survival rate of combination therapy was also increased, with 6 mice surviving (6/9) (Fig. 7E). These data suggested that immune checkpoint inhibitor enhances anti-tumor effect of oncolytic virus and that the combination therapy exhibits potent oncolytic activity.

4. Discussion

OVs selectively replicate in tumor cells and favorably modulate tumor immune microenvironment through a variety of different mechanisms (Chaurasiya et al., 2020; Russell et al., 2019). In this study,

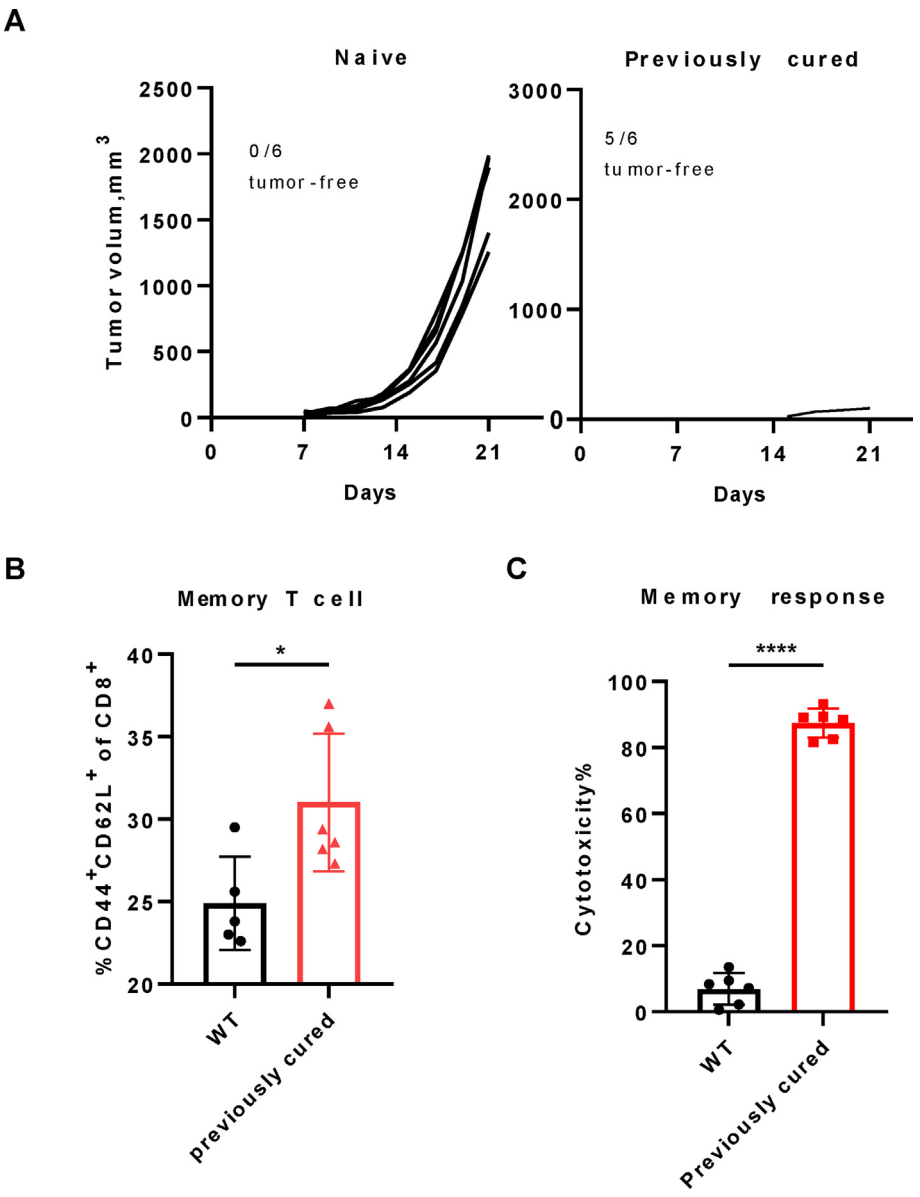

Fig. 5. VSV^{M51R}-Neo-2/15 generates immune memory response against tumor cells. **A** Naive or previously cured mice, which survived for more than 100 days, were subcutaneously rechallenged with 4×10^5 MC-38 cells (n = 6). The volumes of tumor cells post-implantation days were shown. **B** Spleens were isolated from naive or previously cured mice 21 days post MC-38 cell implantation. CD8$^+$ T memory cells from spleen were stained with anti-CD8, anti-CD44 and anti-CD62L. **C** CD8$^+$ T memory cells were isolated from naive or previously cured mice via FACS sorting, and cocultured with MC-38 cells 48 h, cytotoxicity of memory cells was measured by CCK-8 kit. Data are represented as the mean ± SD. Student's *t*-test was used for non-paired comparisons of two groups. *$P < 0.05$; ****$P < 0.0001$.

we engineered a recombinant VSV expressing Neo-2/15, a type of novel IL-2 mimic that lacks CD25 binding site and preferentially activates cytotoxic CD8$^+$ T lymphocytes (Silva et al., 2019). We firstly confirmed the biological activity of Neo-2/15 expressed by VSV^{M51R}-Neo-2/15. The culture medium of infected cells promoted the survival and proliferation of mouse NK cells and CD8$^+$ T cells while it was not effective for Treg cell differentiation *in vitro*. We also did not observe the severe toxicity that commonly occurred in high-dose IL-2 therapy in VSV^{M51R}-Neo-2/15 treatment *in vivo*, which is attributed to the novel molecular design of Neo-2/15 (Silva et al., 2019). Importantly, VSV^{M51R}-Neo-2/15 exhibited better therapeutic effects as evidenced by tumor growth inhibition or survival time in tumor-bearing mice, likely because more CD8$^+$ T cells were induced to control tumor growth. In addition, we found that VSV^{M51R}-Neo-2/15 induced long-term anti-tumor immune memory to resist tumor rechallenge, yet the detailed mechanism remains unknown. It might be very helpful for designing a cancer vaccine if a specific tumor associated antigen is available in future. Our results are in line with a recently published work showing that a recombinant adenovirus Ad5/3-E2F-d24-vIL2, which also carries a variant IL-2, elicits more potent T cells mediated anti-tumor immunity compared to WT IL-2 (Quixabeira et al., 2021). Furthermore, the Ad5/3-E2F-d24-vIL2 appears to induce few suppressive myeloid cells in hamsters bearing pancreatic tumor. However, in present study, the percentage of myeloid-derived suppressor cells was not significantly different between VSV^{M51R}-Neo-2/15 and VSV^{M51R}-mIL-2 groups (Supplementary Fig. S2). It might be due to the different tumor model used in the studies.

Clinical response rates to PD-L1 or PD-1 blocking antibodies correlate with increased PD-L1 expression in tumor tissues (Tumeh et al., 2014). It is of note that VSV^{M51R}-Neo-2/15 infection up-regulates PD-L1

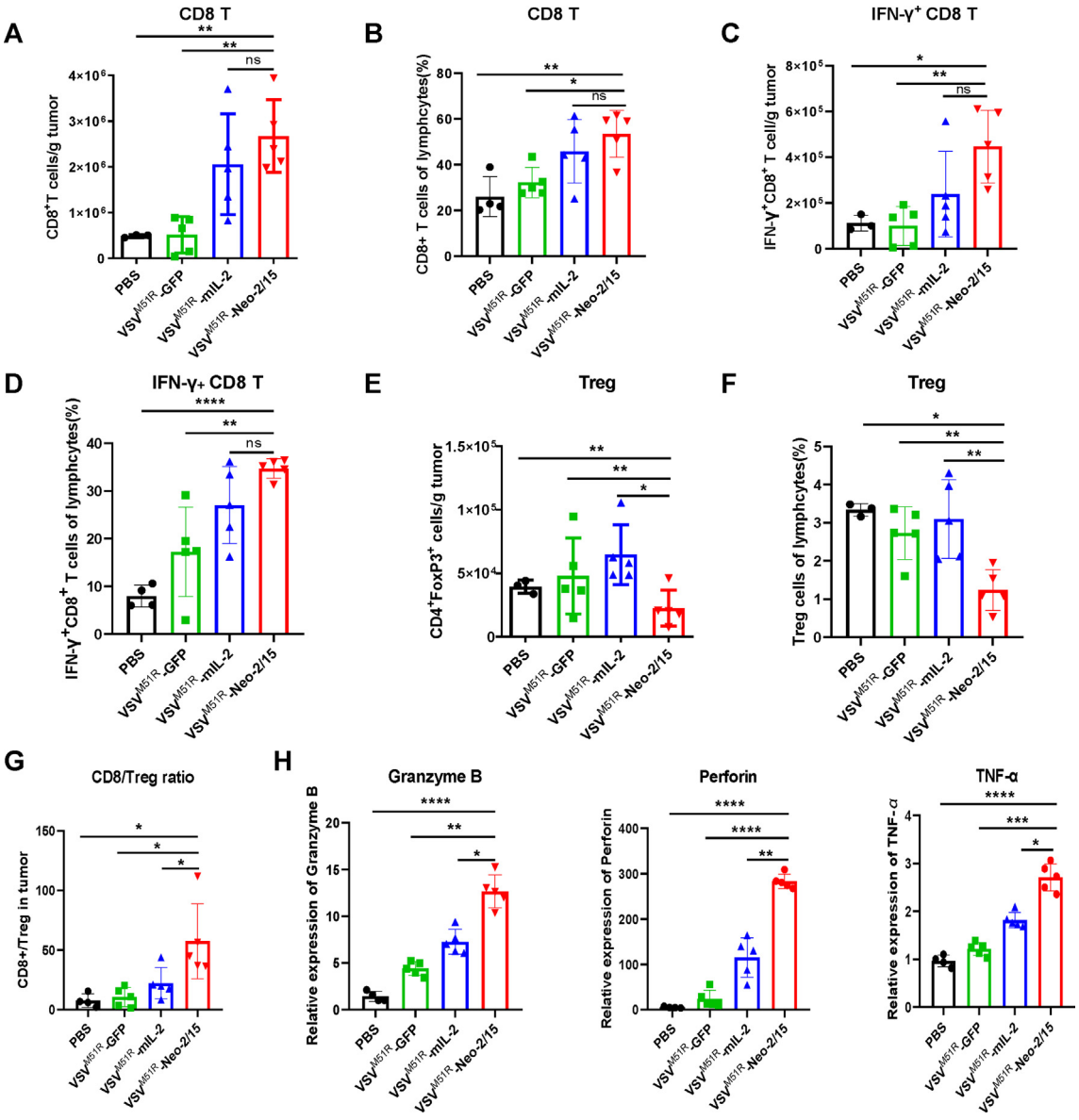

Fig. 6. The change of the tumor infiltration lymphocytes upon VSV^{M51R}-Neo-2/15 therapy. MC-38 cells (7.0×10^5) were implanted into the flank of C57BL/6 mice. When tumor established, mice were subjected to mock treatment (n = 4) or intratumoral injection of 1.0×10^8 pfu VSV^{M51R}-GFP, VSV^{M51R}-mIL-2, VSV^{M51R}-Neo-2/15 (n = 5) every other day and for a total of 3 injections. Tumors were collected the day after the last treatment and tumor infiltration lymphocytes were analyzed by flow cytometry. The absolute number of CD8$^+$ T cells (**A**), IFN-γ$^+$ CD8$^+$ T cells (**C**) and Treg cells (**E**) in tumor of each group were measured. The percentage of CD8$^+$ T cells (**B**), IFN-γ$^+$ CD8$^+$ T (**D**) and Treg cells (**F**) in lymphocytes of each group were measured. The ratio of CD8$^+$ T/Treg (**G**) were measured. MC-38 tumor bearing mice were intratumorally injected with PBS, VSV^{M51R}-GFP, VSV^{M51R}-mIL-2, VSV^{M51R}-Neo-2/15 every two days and for total 3 times. The day after the last injection, CD8$^+$ T cells were sorted from tumors and the total RNA was extracted. The expression of Granzyme B, Perforin, and TNF-α (**H**) were measured by real-time PCR. The relative expressions of these genes in OVs treated groups were normalized with control PBS group. Data are represented as the mean ± SD. One way ANOVA test was used for non-paired comparisons of multiple groups. *$P < 0.05$; **$P < 0.01$; ***$P < 0.001$; ****$P < 0.0001$; ns: no significance.

expression in tumor cells. Previous studies suggest that it is likely to be induced by intratumoral expression of IFN-γ (Abiko et al., 2015; Parker et al., 2016). The combination of VSV^{M51R}-Neo-2/15 with PD-L1 antibody in the study improved the therapeutic effects in mouse model. It might be due to onco-virotherapy increasing the expression level of PD-L1 in tumors and enhancing the therapeutic efficacy of PD-1/PD-L1 blockade. Indeed, we have previously generated a recombinant VSV expressing a single chain anti-PD-L1 antibody that effectively inhibits tumor growth and prolongs survival in mice (Wu et al., 2019). Apart from combining with PD-1/PD-L1 inhibitors, the combination with anti-CTLA-4 antibody (Puzanov et al., 2016) and adoptive T cell therapy (Nishio and Dotti, 2015) also improves the therapeutic efficacy of OVs. Hence, combination immunotherapy may be a promising direction for future cancer treatment.

One of the greatest challenges to effective OV therapy in clinical development is the selection of the optimal method for delivering OVs. At present, intratumoral injection is more widely used than intravenous injection. Direct intratumoral injection can ensure that viral particles reach the lesion directly (Hamid et al., 2020). In other words, it is more targeted and safer. However, there are some concerns that the therapeutic efficacy of local injection may be limited for multiple metastatic tumors. Intravenous injection provides an opportunity for the virus to reach all tumor lesions, while its bioavailability is poor. Intravenously administered viruses are susceptible to be cleared by circulating

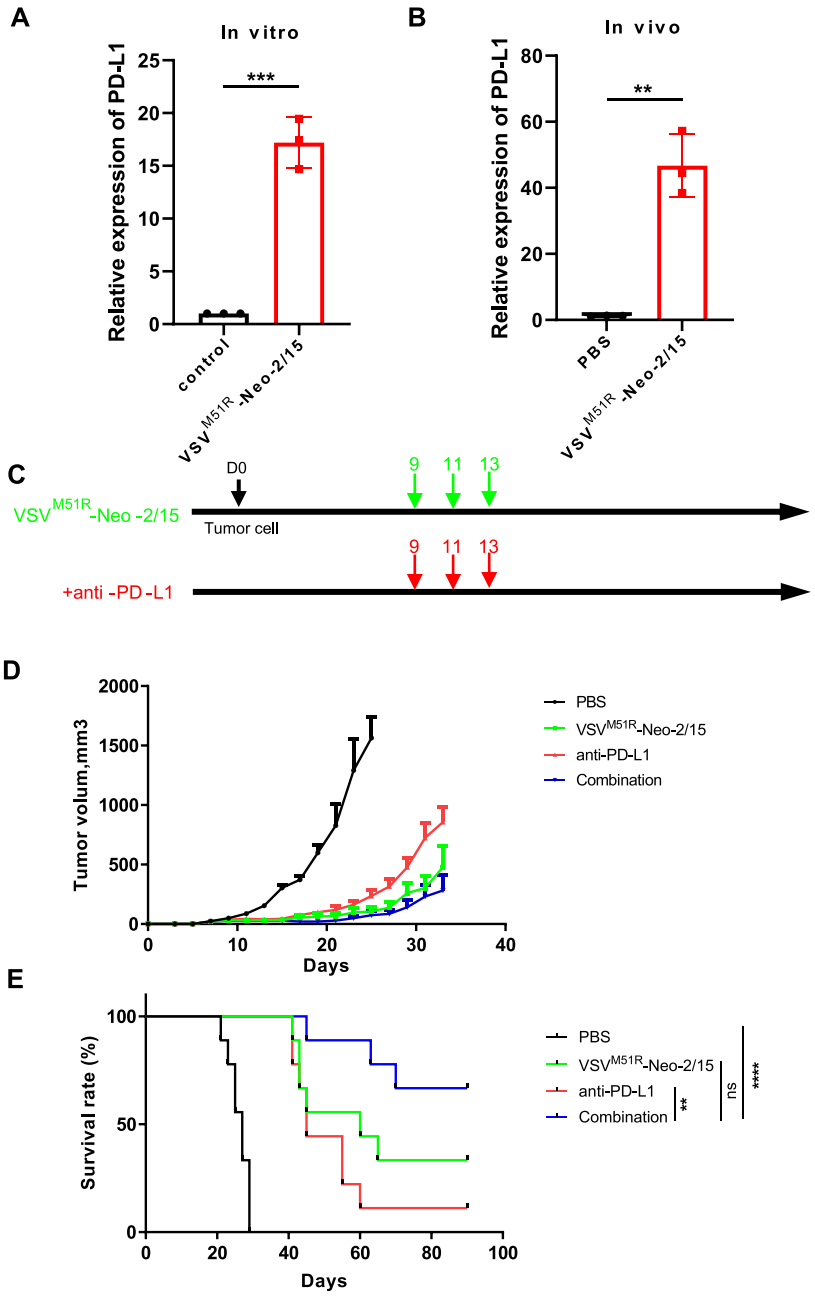

Fig. 7. Immune checkpoint inhibitor enhances therapeutic effects of VSV^{M51R}-Neo-2/15. VSV^{M51R}-Neo-2/15 infected MC-38 cells (**A**) and virus-injected tumors (**B**) were collected and analyzed using real-time PCR to determine the expression of PD-L1. **C** MC-38 cells (7.0×10^5) were implanted into the flank of C57BL/6 mice. When tumors reached an average volume of 50 mm^3, mice were either intratumorally injected with 1.0×10^8 pfu VSV^{M51R}-Neo-2/15 or intraperitoneally injected with 100 μg anti-PD-L1 antibody (n = 9) on day 9, every two days and for total 3 times. Mice in combination group were treated with 1.0×10^8 pfu VSV^{M51R}-Neo-2/15 (intratumorally) and 100 μg anti-PD-L1 Ab (intraperitoneally) on day 9 (n = 9). **D** The average tumor volume per group was determined every 2 days. **E** The survival rate of each group. Data are represented as the mean ± SD. Student's *t*-test was used for non-paired comparisons of two groups. The Kaplan-Meier method with the log-rank test was used for survival analysis. $^{**}P < 0.01$; $^{***}P < 0.001$; ns: no significance.

complements or antibodies (Russell et al., 2012). The systemic effect of OV therapy previously has been observed in several studies including VSV (Patel et al., 2015; Wang et al., 2020; Nakatake et al., 2021), therefore we believe that VSV^{M51R}-Neo-2/15 local administration could inhibit not only the infected tumors, but also the non-injected distant tumors, supporting the potential of VSV^{M51R}-Neo-2/15 in treating in metastatic lesions. We speculate that the activated immune cells are capable to enter blood circulation and reach distant tumor tissues. However, intratumoral delivery still has its limitations in clinical application because interventional surgery is not feasible in many cancers.

5. Conclusions

In summary, we demonstrated that a recombinant VSV expressing Neo-2/15 was able to efficiently augment anti-tumor immune responses, which retarded tumor growth and protected against tumor recurrence,

and the therapeutic effect was further enhanced with immune checkpoint inhibitor, thereby providing a new valid therapeutic potential for cancer patients.

Data availability

All data relevant to the study are included in the article or uploaded as supplementary information.

Ethics statement

All animal experiments were performed in accordance with the guidelines for the Care and Use of Laboratory Animals, Ministry of Health, China (1998), and the protocols used were approved by the Ethics Committee of Soochow University.

Author contributions

Manman Wu: conceptualization, investigation, data curation, methodology, formal analysis, writing–original draft. Yiwei Wang: investigation and data curation. Chuanjian Wu: investigation and data curation. Huang Huang: investigation and data curation. Xinyuan Zhou: method ology, formal analysis. Jun Wang: investigation, formal analysis and funding acquisition. Sidong Xiong: conceptualization, formal analysis and funding acquisition. Chunsheng Dong: conceptualization, supervision, formal analysis, writing–original draft and funding acquisition.

Conflict of interest

The authors declare that they have no conflict of interest.

Acknowledgements

We thank Dr. John Rose at Yale University for providing VSV reverse genetic system. This work was supported by the National Natural Science Foundation of China Grants 31870867, 32170148, 31970844, 32170927, 32170914 and 82101848, and by the Jiangsu Provincial Innovative Research Team, the Priority Academic Program Development of Jiangsu Higher Education Institutions.

Appendix A. Supplementary data

Supplementary data to this article can be found online at https://doi.org/10.1016/j.virs.2024.09.007.

References

Abbas, A.K., Trotta, E., D, R.S., Marson, A., Bluestone, J.A., 2018. Revisiting IL-2: biology and therapeutic prospects. Sci Immunol 3 (25), eaat1482.
Abiko, K., Matsumura, N., Hamanishi, J., Horikawa, N., Murakami, R., Yamaguchi, K., Yoshioka, Y., Baba, T., Konishi, I., Mandai, M., 2015. IFN-gamma from lymphocytes induces PD-L1 expression and promotes progression of ovarian cancer. Br. J. Cancer 112, 1501–1509.
Ahmadzadeh, M., Rosenberg, S.A., 2006. IL-2 administration increases CD4+ CD25(hi) Foxp3+ regulatory T cells in cancer patients. Blood 107, 2409–2414.
Ahmed, M., Puckett, S., Lyles, D.S., 2010. Susceptibility of breast cancer cells to an oncolytic matrix (M) protein mutant of vesicular stomatitis virus. Cancer Gene Ther. 17, 883–892.
Amedei, A., Prisco, D., Mm, D.E., 2013. The use of cytokines and chemokines in the cancer immunotherapy. Recent Pat. Anti-Cancer Drug Discov. 8, 126–142.
Bishnoi, S., Tiwari, R., Gupta, S., Byrareddy, S.N., Nayak, D., 2018. Oncotargeting by Vesicular stomatitis Virus (VSV): advances in Cancer therapy. Viruses 10, 90.
Blattman, J.N., Grayson, J.M., Wherry, E.J., Kaech, S.M., Smith, K.A., Ahmed, R., 2003. Therapeutic use of IL-2 to enhance antiviral T-cell responses in vivo. Nat. Med. 9, 540–547.
Boyman, O., Sprent, J., 2012. The role of interleukin-2 during homeostasis and activation of the immune system. Nat. Rev. Immunol. 12, 180–190.
Cary, Z.D., Willingham, M.C., Lyles, D.S., 2011. Oncolytic vesicular stomatitis virus induces apoptosis in U87 glioblastoma cells by a type II death receptor mechanism and induces cell death and tumor clearance in vivo. J. Virol. 85, 5708–5717.
Chaurasiya, S., Chen, N.G., Fong, Y., 2018. Oncolytic viruses and immunity. Curr. Opin. Immunol. 51, 83–90.
Chaurasiya, S., Yang, A., Kang, S., Lu, J., Kim, S.I., Park, A.K., Sivanandam, V., Zhang, Z., Woo, Y., Warner, S.G., Fong, Y., 2020. Oncolytic poxvirus CF33-hNIS-DeltaF14.5 favorably modulates tumor immune microenvironment and works synergistically with anti-PD-L1 antibody in a triple-negative breast cancer model. OncoImmunology 9, 1729300.
Ebert, O., Shinozaki, K., Huang, T.G., Savontaus, M.J., Garcia-Sastre, A., Woo, S.L., 2003. Oncolytic vesicular stomatitis virus for treatment of orthotopic hepatocellular carcinoma in immune-competent rats. Cancer Res. 63, 3605–3611.
Galivo, F., Diaz, R.M., Thanarajasingam, U., Jevremovic, D., Wongthida, P., Thompson, J., Kottke, T., Barber, G.N., Melcher, A., Vile, R.G., 2010. Interference of CD40L-mediated tumor immunotherapy by oncolytic vesicular stomatitis virus. Hum. Gene Ther. 21, 439–450.
Goradel, N.H., Baker, A.T., Arashkia, A., Ebrahimi, N., Ghorghanlu, S., Negahdari, B., 2021. Oncolytic virotherapy: challenges and solutions. Curr. Probl. Cancer 45, 100639.
Gray, Z., Tabarraei, A., Moradi, A., Kalani, M.R., 2019. M51R and Delta-M51 matrix protein of the vesicular stomatitis virus induce apoptosis in colorectal cancer cells. Mol. Biol. Rep. 46, 3371–3379.
Hamid, O., Ismail, R., Puzanov, I., 2020. Intratumoral immunotherapy-update 2019. Oncol. 25, e423–e438.
Harrington, K., Freeman, D.J., Kelly, B., Harper, J., Soria, J.C., 2019. Optimizing oncolytic virotherapy in cancer treatment. Nat. Rev. Drug Discov. 18, 689–706.
Johnson, D.B., Puzanov, I., Kelley, M.C., 2015. Talimogene laherparepvec (T-VEC) for the treatment of advanced melanoma. Immunotherapy 7, 611–619.
Lamers, C.H., Sleijfer, S., van Steenbergen, S., van Elzakker, P., van Krimpen, B., Groot, C., Vulto, A., Den Bakker, M., Oosterwijk, E., Debets, R., Gratama, J.W., 2013. Treatment of metastatic renal cell carcinoma with CAIX CAR-engineered T cells: clinical evaluation and management of on-target toxicity. Mol. Ther. 21, 904–912.
Lawson, N.D., Stillman, E.A., Whitt, M.A., Rose, J.K., 1995. Recombinant vesicular stomatitis viruses from DNA. Proc. Natl. Acad. Sci. USA 92, 4477–4481.
Li, Y., Li, Y.F., Si, C.Z., Zhu, Y.H., Jin, Y., Zhu, T.T., Liu, M.Y., Liu, G.Y., 2016. CCL21/IL21-armed oncolytic adenovirus enhances antitumor activity against TERT-positive tumor cells. Virus Res. 220, 172–178.
Lin, H., Wei, S., Hurt, E.M., Green, M.D., Zhao, L., Vatan, L., Szeliga, W., Herbst, R., Harms, P.W., Fecher, L.A., Vats, P., Chinnaiyan, A.M., Lao, C.D., Lawrence, T.S., Wicha, M., Hamanishi, J., Mandai, M., Kryczek, I., Zou, W., 2018. Host expression of PD-L1 determines efficacy of PD-L1 pathway blockade-mediated tumor regression. J. Clin. Invest. 128, 805–815.
Marabondo, S., Kaufman, H.L., 2017. High-dose interleukin-2 (IL-2) for the treatment of melanoma: safety considerations and future directions. Expet Opin. Drug Saf. 16, 1347–1357.
Markert, J.M., Cody, J.J., Parker, J.N., Coleman, J.M., Price, K.H., Kern, E.R., Quenelle, D.C., Lakeman, A.D., Schoeb, T.R., Palmer, C.A., Cartner, S.C., Gillespie, G.Y., Whitley, R.J., 2012. Preclinical evaluation of a genetically engineered herpes simplex virus expressing interleukin-12. J. Virol. 86, 5304–5313.
Michot, J.M., Bigenwald, C., Champiat, S., Collins, M., Carbonnel, F., Postel-Vinay, S., Berdelou, A., Varga, A., Bahleda, R., Hollebecque, A., Massard, C., Fuerea, A., Ribrag, V., Gazzah, A., Armand, J.P., Amellal, N., Angevin, E., Noel, N., Boutros, C., Mateus, C., Robert, C., Soria, J.C., Marabelle, A., Lambotte, O., 2016. Immune-related adverse events with immune checkpoint blockade: a comprehensive review. Eur. J. Cancer 54, 139–148.
Morgan, D.A., Ruscetti, F.W., Gallo, R., 1976. Selective in vitro growth of T lymphocytes from normal human bone marrows. Science 193, 1007–1008.
Nakatake, M., Kuwano, N., Kaitsurumaru, E., Kurosaki, H., Nakamura, T., 2021. Fusogenic oncolytic vaccinia virus enhances systemic antitumor immune response by modulating the tumor microenvironment. Mol. Ther. 29, 1782–1793.
Nishio, N., Dotti, G., 2015. Oncolytic virus expressing RANTES and IL-15 enhances function of CAR-modified T cells in solid tumors. OncoImmunology 4, e988098.
Parker, B.S., Rautela, J., Hertzog, P.J., 2016. Antitumour actions of interferons: implications for cancer therapy. Nat. Rev. Cancer 16, 131–144.
Patel, M.R., Jacobson, B.A., Ji, Y., Drees, J., Tang, S., Xiong, K., Wang, H., Prigge, J.E., Dash, A.S., Kratzke, A.K., Mesev, E., Etchison, R., Federspiel, M.J., Russell, S.J., Kratzke, R.A., 2015. Vesicular stomatitis virus expressing interferon-beta is oncolytic and promotes antitumor immune responses in a syngeneic murine model of non-small cell lung cancer. Oncotarget 6, 33165–33177.
Puzanov, I., Milhem, M.M., Minor, D., Hamid, O., Li, A., Chen, L., Chastain, M., Gorski, K.S., Anderson, A., Chou, J., Kaufman, H.L., Andtbacka, R.H., 2016. Talimogene laherparepvec in combination with ipilimumab in previously untreated, unresectable stage IIIB-IV melanoma. J. Clin. Oncol. 34, 2619–2626.
Quixabeira, D.C.A., Zafar, S., Santos, J.M., Cervera-Carrascon, V., Havunen, R., Kudling, T.V., Basnet, S., Anttila, M., Kanerva, A., Hemminki, A., 2021. Oncolytic adenovirus coding for a variant interleukin 2 (vIL-2) cytokine Re-programs the tumor microenvironment and confers enhanced tumor control. Front. Immunol. 12, 674400.
Restifo, N.P., Dudley, M.E., Rosenberg, S.A., 2012. Adoptive immunotherapy for cancer: harnessing the T cell response. Nat. Rev. Immunol. 12, 269–281.
Rosenberg, S.A., 2001. Progress in human tumour immunology and immunotherapy. Nature 411, 380–384.
Rosenberg, S.A., Restifo, N.P., 2015. Adoptive cell transfer as personalized immunotherapy for human cancer. Science 348, 62–68.

Russell, L., Peng, K.W., Russell, S.J., Diaz, R.M., 2019. Oncolytic viruses: priming time for cancer immunotherapy. BioDrugs 33, 485–501.
Russell, S.J., Peng, K.W., Bell, J.C., 2012. Oncolytic virotherapy. Nat. Biotechnol. 30, 658–670.
Sharma, M., Khong, H., Fa'Ak, F., Bentebibel, S.E., Janssen, L.M.E., Chesson, B.C., Creasy, C.A., Forget, M.A., Kahn, L.M.S., Pazdrak, B., Karki, B., Hailemichael, Y., Singh, M., Vianden, C., Vennam, S., Bharadwaj, U., Tweardy, D.J., Haymaker, C., Bernatchez, C., Huang, S., Rajapakshe, K., Coarfa, C., Hurwitz, M.E., Sznol, M., Hwu, P., Hoch, U., Addepalli, M., Charych, D.H., Zalevsky, J., Diab, A., Overwijk, W.W., 2020. Bempegaldesleukin selectively depletes intratumoral Tregs and potentiates T cell-mediated cancer therapy. Nat. Commun. 11, 661.
Siegel, J.P., Puri, R.K., 1991. Interleukin-2 toxicity. J. Clin. Oncol. 9, 694–704.
Silva, D.A., Yu, S., Ulge, U.Y., Spangler, J.B., Jude, K.M., Labao-Almeida, C., Ali, L.R., Quijano-Rubio, A., Ruterbusch, M., Leung, I., Biary, T., Crowley, S.J., Marcos, E., Walkey, C.D., Weitzner, B.D., Pardo-Avila, F., Castellanos, J., Carter, L., Stewart, L., Riddell, S.R., Pepper, M., Bernardes, G.J.L., Dougan, M., Garcia, K.C., Baker, D., 2019. De novo design of potent and selective mimics of IL-2 and IL-15. Nature 565, 186–191.
Stojdl, D.F., Lichty, B., Knowles, S., Marius, R., Atkins, H., Sonenberg, N., Bell, J.C., 2000. Exploiting tumor-specific defects in the interferon pathway with a previously unknown oncolytic virus. Nat. Med. 6, 821–825.
Togashi, Y., Shitara, K., Nishikawa, H., 2019. Regulatory T cells in cancer immunosuppression - implications for anticancer therapy. Nat. Rev. Clin. Oncol. 16, 356–371.
Topalian, S.L., Drake, C.G., Pardoll, D.M., 2015. Immune checkpoint blockade: a common denominator approach to cancer therapy. Cancer Cell 27, 450–461.
Tumeh, P.C., Harview, C.L., Yearley, J.H., Shintaku, I.P., Taylor, E.J., Robert, L., Chmielowski, B., Spasic, M., Henry, G., Ciobanu, V., West, A.N., Carmona, M., Kivork, C., Seja, E., Cherry, G., Gutierrez, A.J., Grogan, T.R., Mateus, C., Tomasic, G., Glaspy, J.A., Emerson, R.O., Robins, H., Pierce, R.H., Elashoff, D.A., Robert, C., Ribas, A., 2014. PD-1 blockade induces responses by inhibiting adaptive immune resistance. Nature 515, 568–571.
Udayakumar, T.S., Betancourt, D.M., Ahmad, A., Tao, W., Totiger, T.M., Patel, M., Marples, B., Barber, G., Pollack, A., 2020. Radiation attenuates prostate tumor antiviral responses to vesicular stomatitis virus containing IFNbeta, resulting in pronounced antitumor systemic immune responses. Mol. Cancer Res. 18, 1232–1243.
Wang, G., Kang, X., Chen, K.S., Jehng, T., Jones, L., Chen, J., Huang, X.F., Chen, S.Y., 2020. An engineered oncolytic virus expressing PD-L1 inhibitors activates tumor neoantigen-specific T cell responses. Nat. Commun. 11, 1395.
Wang, X., Rickert, M., Garcia, K.C., 2005. Structure of the quaternary complex of interleukin-2 with its alpha, beta, and gammac receptors. Science 310, 1159–1163.
Wu, C., Wu, M., Liang, M., Xiong, S., Dong, C., 2019. A novel oncolytic virus engineered with PD-L1 scFv effectively inhibits tumor growth in a mouse model. Cell. Mol. Immunol. 16, 780–782.
Ylosmaki, E., Ylosmaki, L., Fusciello, M., Martins, B., Ahokas, P., Cojoc, H., Uoti, A., Feola, S., Kreutzman, A., Ranki, T., Karbach, J., Viitala, T., Priha, P., Jager, E., Pesonen, S., Cerullo, V., 2021. Characterization of a novel OX40 ligand and CD40 ligand-expressing oncolytic adenovirus used in the PeptiCRAd cancer vaccine platform. Mol Ther Oncolytics 20, 459–469.